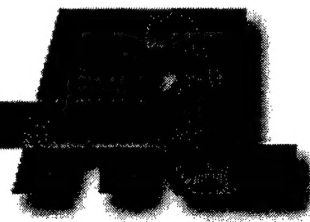


ARMY RESEARCH LABORATORY



# Generation of Polymer Nanofibers Through Electrospinning

Joseph Deitzel  
Nora C. Beck Tan  
James D. Kleinmeyer  
Joseph Rehrmann  
David Tevault  
Darrell Reneker  
Ibrahim Sendijarevic  
Anthony McHugh

ARL-TR-1989

JUNE 1999

19990722 074

DTIC QUALITY INSPECTED 4

Approved for public release; distribution is unlimited.

Kevlar® is a registered trademark of E.I. DuPont de Nemours & Co., Inc.

The findings in this report are not to be construed as an official Department of the Army position  
unless so designated by other authorized documents.

Citation of manufacturer's or trade names does not constitute an official endorsement or approval of  
the use thereof.

Destroy this report when it is no longer needed. Do not return it to the originator.

# **Army Research Laboratory**

Aberdeen Proving Ground, MD 21005-5066

---

---

ARL-TR-1989

June 1999

---

## **Generation of Polymer Nanofibers Through Electrospinning**

Joseph M. Deitzel  
Nora C. Beck Tan  
James D. Kleinmeyer  
Weapons & Materials Research Directorate, ARL

Joseph Rehrmann  
David Tevault  
Edgewood Chemical-Biological Center

Darrell Reneker  
University of Akron

Ibrahim Sendijarevic  
Anthony McHugh  
University of Illinois

---

---

Approved for public release; distribution is unlimited.

---

---

---

## Abstract

---

Non-woven fabrics composed of nanofibers have a large specific surface area and small pore size compared to commercial textiles. These properties make such non-woven fabrics excellent candidates for filter and membrane applications, particularly in the areas of chemical and biological agent defense. Nanofibers may be produced by electrospinning, which uses an electric field to produce continuous fibers with diameters in the tens of nanometers range. Although the technique has been known for some time, very little information concerning the effect of processing variables such as solution concentration, viscosity, surface tension, flow rate and acceleration voltage on final fiber properties exists in the literature. In this work, nanofibers of polyethylene oxide have been electrospun from a range of solution concentrations and for a range of voltages. Wide angle X-ray diffraction and differential scanning calorimetry indicate that crystal structure is poorly developed in the electrospun fibers, when compared to results obtained from poly(ethylene oxide) powder. Fiber diameter increases with increasing concentration by the 0.53 power. We find that for concentrations of 8% (wt) and greater, a bimodal fiber diameter distribution has been observed, which is analogous to results reported for electrospray experiments. The density of node defects has been shown to increase with increasing voltage for a constant solution feed rate.

## TABLE OF CONTENTS

	<u>Page</u>
LIST OF FIGURES .....	v
1. MOTIVATION FOR RESEARCH.....	1
1.1 Technical Background .....	2
2. EXPERIMENTAL .....	6
3. RESULTS AND DISCUSSION .....	8
3.1 Nanofiber Morphology: Voltage Dependence .....	8
3.2 Nanofiber Morphology: Concentration Dependence .....	14
3.3 General Characteristics of Electrospun Fibers and Fiber Mats .....	19
4. CONCLUSIONS .....	24
REFERENCES.....	27
DISTRIBUTION LIST .....	29
REPORT DOCUMENTATION PAGE .....	33

**INTENTIONALLY LEFT BLANK**

## LIST OF FIGURES

<u>Figure</u>	<u>Page</u>
1. Electrospinning/Electrospray Process .....	3
2. Electrospinning Current as a Function of Voltage .....	9
3. Initiating Cone and Corresponding Fiber Mat for a 7% PEO-Water Solution Spun at 5.5 kV .....	10
4. Initiating Cone and Corresponding Fiber Mat for a 7% PEO-Water Solution Spun at 7.0 kV .....	11
5. Initiating Cone and Corresponding Fiber Mat for a 7% PEO-Water Solution Spun at 9.0 kV .....	12
6. Node Density as a Function of Electrospinning Voltage .....	13
7. Concentration Dependence of Solution Surface Tension and Solution Viscosity for PEO-Water Solutions .....	15
8. Electron Micrographs of Fiber Mats Electrospun From 4%, 7%, and 10% PEO- Water Solutions .....	16
9. Average Fiber Diameter as a Function of PEO Concentration .....	16
10. Bimodal Distribution of Fiber Diameters Electrospun From 7% and 10% PEO- Water Solution .....	17
11. Percentage of Secondary Distribution as a Function of Concentration .....	18
12. High Speed Photo-micrographs of the Electrospinning Process for 4% and 10% Solution Concentrations .....	18
13. Specific Surface Area as a Function of Concentration .....	19
14. WAXD Patterns for PEO Powder and PEO Fiber Mat Electrospun From 10% PEO-Water Solution .....	20
15. Fiber Mats Electrospun From 10% Solution of PEO in Water Collected Onto an Aluminum Screen .....	21
16. 7% Solution of 100,000 Mol. Wt. PEO in Water Electrosprayed Onto an Aluminum Grid .....	22
17. Photomicrograph of 2% PEO-Water Electrospun Onto an Aluminum Grid .....	23
18. Three-dimensional Structure in Non-woven Fiber Mat Electrospun From a 7% Solution of 400,000 Mol. Wt. PEO and Water Electrospun at 11 kV Onto a Cloth Substrate .....	23
19. High Magnification Images of Figure 18 at Different Working Distances .....	24

INTENTIONALLY LEFT BLANK

## GENERATION OF POLYMER NANOFIBERS THROUGH ELECTROSPINNING

### 1. MOTIVATION FOR RESEARCH

Polymer fibers are used in a wide variety of military and civilian applications, including textiles and composite reinforcement. Traditional methods of obtaining polymer fibers include melt spinning [1], spinning from solution, and spinning from the gel state.[2] Typical fiber diameters obtained from these methods range from 5 to 500 microns in size. The lower limit of fiber diameter that is consistently achievable by these methods is on the order of magnitude of a micron. Recently [3], there has been increased interest in another method of fiber production, electrospinning, which can consistently produce fibers that are sub-micron in diameter. Textiles produced from these fibers are showing promise for exploitation in filtration applications.

In military applications, current filter technology employs either activated carbon or zeolite particles that achieve ultra high surface area through porosity. Because of their granular nature, these materials restrict the design of filters used in chemical and biological warfare agent defense for both personal and vehicular applications. In order to be effective, the particles that comprise these materials must remain in a densely packed configuration. This is achieved by using a polymer binder and applying a constant pressure on the filter material. However, the need to apply a constant pressure restricts the design of the filter shape, and the use of polymer binder reduces effective surface area and often reduces gas throughput. A further problem associated with these porous filter materials is that it is often difficult to chemically modify all the available surface area with sites designed to neutralize warfare agents.

These problems could be addressed by the use of filters composed of non-woven polymer fiber mats, but the total specific surface area associated with commercial filters of this type is considerably less than that of activated carbon or zeolite filters. However, non-woven fiber mats composed of electrospun fibers process will have a much higher specific surface area than current commercial, non-woven fiber mat filters because of the small diameter of the fibers. In addition, it should be possible to electrospin fibers from polymers with specific functional groups that can be made to segregate on the fiber surface with a minimum of effort. In this manner, all the available surface area can be chemically modified to neutralize chemical/biological agents. These factors make electrospun non-woven fiber mats perfect candidates for military filter applications.

The advantages of electrospun non-woven fiber mats that have been discussed for filter applications also make these materials excellent candidates for soldier's protective clothing.[3] A major problem with current protective clothing is that barrier materials designed to keep warfare

agents out also prevent the evaporation of perspiration. One method to address this problem is to use nanoporous fluoro-polymer membranes, which wick perspiration away from the body. However, these membranes are expensive. By using electrospinning technology, which provides non-woven fabrics with a large specific surface area and small pore size, it should be possible to produce fabrics with properties similar to these fluoro-polymer membranes at a much cheaper cost.

### 1.1 Technical Background

It has been understood for most of this century that it is possible to use electrostatic fields to form and accelerate liquid jets from the tip of a capillary.[4,5,6] A hemispherical meniscus of liquid suspended in equilibrium at the end of a capillary will be distorted into a conical shape in the presence of an electric field. A balancing of the repulsive force resulting from the induced charge distribution on the surface of the meniscus with the surface tension of the liquid causes this distortion. In 1964, Taylor [5] showed that for a critical voltage, the equilibrium shape of a suspended meniscus was a cone with a semi-vertical angle of  $49.3^\circ$ . When this critical voltage is exceeded, a stable jet of liquid is ejected from the cone tip. In the case of low viscosity liquids, the jet disintegrates into droplets as a result of surface tension. For high viscosity liquids, the jet does not disintegrate; it simply hits the grounded target.[6] The first case is known as electrospraying and it is used in many industries to obtain aerosols with narrow distributions of sub-micron drops. When applied to polymer solutions and melts, the second case is known as electrospinning and it generates polymer fibers that are sub-micron in diameter. For the discussion of the results presented in this report, it will be necessary to explore each of these cases in more detail.

In the case of electrospray, when the jet is accelerated away from the cone apex, it decreases in diameter and disintegrates into droplets. As these drops continue to accelerate away from the cone tip, their diameter decreases as a result of evaporation. When the drop diameter decreases, the surface charge density increases until it exceeds a maximum value. At that point, the drop undergoes Coulombic fission, producing numerous smaller drops. This process is continued repeatedly until the grounded target is reached (see Figure 1). When the liquid that is used is a low viscosity solution of something such as pigment, it is possible to get a narrow distribution of sub-micron particles using this process. In the last 10 years, there has been significant interest in the electrospray technique which allows the production of monodispersed droplets that range in size from tens of microns to tens of nanometers, depending on initial

conditions. This technique has a wide variety of applications ranging from ink jet printers to fuel injection systems.[7,8]

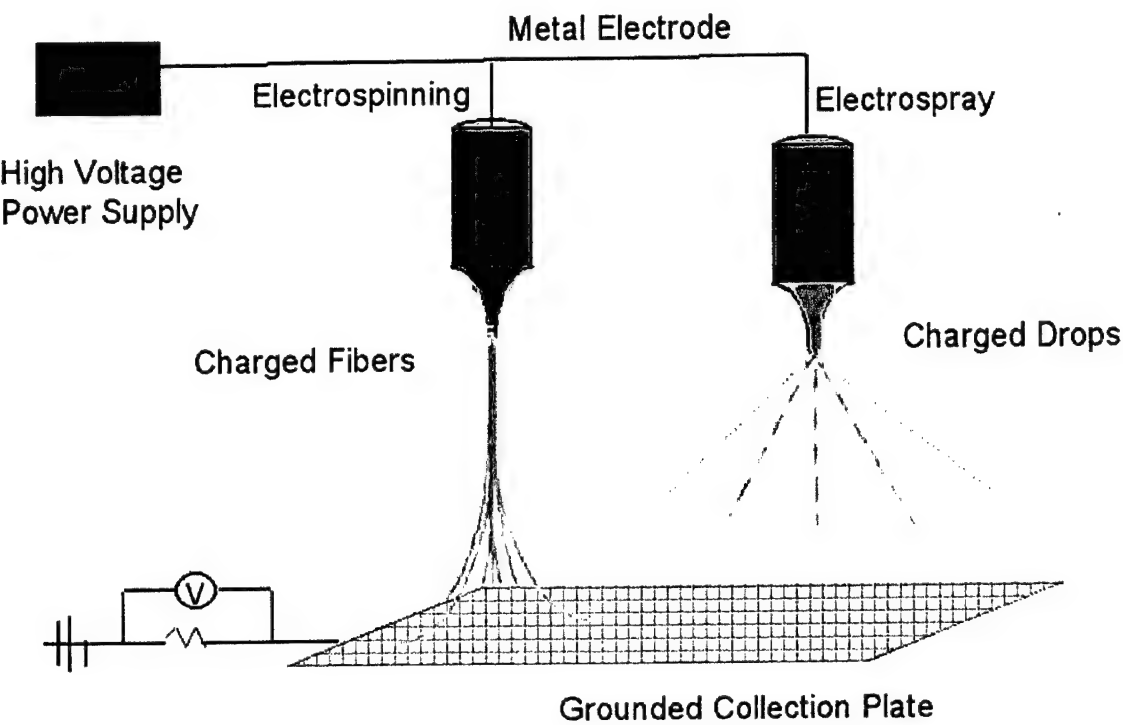


Figure 1. Electrospraying/Electrospinning Process.

There are two review articles, one by Cloupeau and Prunet-Foch [7] and the other by Grace and Marijnissen [8] that discuss the effects of process variables in electrospray such as solution concentration, conductivity, flow rate, and acceleration voltage on droplet size and distribution. The major emphasis in these two articles is the identification of different modes of jet formation. These modes are characterized by varying degrees of instability associated with the initiating jet at the tip of the capillary and are achieved by manipulating the flow rate of solution to the capillary tip and the applied voltage.

One key point made by both reviews is that different modes yield different drop diameters and diameter size distributions. This is important because numerous papers report apparently conflicting data that in reality are the result of spraying from different modes. In order to compare data, one must first understand from which mode the electrospray jet is being initiated. For a given flow rate, the first mode observed by most authors is the dripping mode. This is the case when gravity is the dominant force acting on the initial drop. The initial drop diameter

before it detaches from the capillary tip is characteristically larger than the diameter of the capillary. As voltage is applied and increased, the frequency of the drops increases while the diameter of the individual drops decreases. This is because the electrostatic force on the drop decreases the “apparent” surface tension of the liquid in the drop. It has also been observed that for a given flow rate in this mode, reduction of the capillary diameter results in an increase in drop frequency and a decrease in drop size. Chen and Prui [9] have observed that the current carried to ground by the drops also increases with increasing voltage in this electrospray mode.

At some point as the voltage is increased, a transition mode is encountered that is designated the “pulsating mode.” In this mode, the initiating jet at the end of the capillary alternates from a hemispherical shape to a conical shape. This mode results in a broad droplet size distribution, and the measured current carried to ground is essentially constant. This mode is stable for a large voltage range in comparison to other modes that are observed. Further increases in the voltage will result in the mode described in detail by Taylor, and is known as the Taylor cone [6], or cone-jet mode.[9] It is discussed in more detail in the next paragraph. Multiple jets can form when the voltage is further increased, and finally the jet will disappear and material will spatter as the maximum practical voltage is reached. This is generally accompanied by consistent dielectric disintegration of the ambient atmosphere.

The cone-jet mode is the mode of greatest interest to the electrospray community. It is characterized by a cone-shaped drop of liquid suspended at the capillary tip, with a jet of solution emitted from the apex of the cone. The length of this jet is directly proportional to voltage. The jet of solution decreases in diameter as it travels away from the tip of the capillary. At some point, the diameter becomes small enough that it disintegrates into droplets as a result of varicose instabilities. As shown by Gomez and Tang [10], the disintegration of the jet results in a bimodal distribution of large, primary droplets and small satellite drops. Because of their small size, these satellite drops are driven to the periphery of the spray cone by the local electric fields of the larger droplets. The result is a core-shell structure of the spray cone, with small satellite droplets on the outside and larger primary drops on the inside. Monodispersed particle sizes can be obtained by collecting only the primary core droplets and excluding the smaller satellite drops. In an earlier study, Gomez and Tang [11] demonstrated that these primary droplets underwent fission, producing smaller, equal-sized daughter droplets. It is this process that generates drop sizes in the submicron region.

For the specific case of the cone-jet mode, the average droplet size decreases while the droplet frequency increases if the flow rate is decreased or the solution conductivity increases.

The current that is carried to the ground increases as the transition from the pulsed mode to the cone-jet mode is made. Specifically, Chen, Pui, and Kaufman [9] demonstrated that the drop size,  $D_d$ , scaled as  $(Q/K)^{1/3}$ , in which  $Q$  is the flow rate and  $K$  is the conductivity of the solution. This confirmed the work of Fernandez de la Mora and Loscertales [12] as well as Ganan-Calvo [13], who also developed empirical scaling laws to the  $1/3$  power. Other investigators showed that the electrospray current scaled with  $(QK)^{1/2}$  during some circumstances. Both sets of observations were made with sugar solutions whose viscosity, relative permittivity, and surface tension were kept constant.

A final experiment looked at the effect on concentration with respect to drop size. It was observed that the drop size increased by a power of  $1/3$  with increasing concentration. It was also seen that as the concentration increased, the drop size distribution became bimodal in nature. As a possible explanation for the existence of a bimodal distribution, it was suggested that the distribution peak corresponding to the smaller diameter represented satellite drops formed during the initial disintegration of the solution jet. However, further investigation is needed to confirm this theory.

If the electrospray process is applied to a polymer solution of sufficient concentration, the initial jet will not disintegrate into drops as a result of varicose instabilities. Instead, the solvent will evaporate as the jet proceeds to the target, leaving polymer fiber. This is known as the electrospinning process. Not as much attention has been given to characterization of the electrospinning process as to the electrospray process. This is most likely because of the perceived lack of possible applications. However, interest in the electrospinning process has increased in recent years [14,15,16]. In 1971, Baumgarten [17] studied the effects of various processing variables on the production of acrylic resin fibers electrospun from Dimethylformamide (DMF). He looked at a range of concentrations from 7.5% to 20%, whose viscosities ranged from 1.7 to 215.0 poise. It was observed that increasing viscosity resulted in an increase in the fiber diameter. The diameter increased by a power of  $\sim 0.5$  over the range of viscosities. Fiber diameters associated with different viscosities were obtained by averaging 25 measurements taken from electron micrographs. It was also observed that the initiating jet at the capillary tip changed from a hemispherical shape to a conical shape as the viscosity increased. The jet length before the onset of instability was also observed to increase with viscosity.

Note that it was determined, based on microflash photographs of the spinning process, that for this system a single fiber was being produced in a normal atmosphere. Subsequent data analysis and interpretation were based on the idea that a single polymer filament was being produced. However, when spinning was performed in a Freon-12 atmosphere, small fiber

“offshoots” from the main fiber were observed. It was noted that these offshoots occurred at sharp bends in the main fiber. More recently, Reneker [14,15,16] reported this offshoot, or splaying, phenomenon in ambient conditions; he also reported observing a single filament jet. It is not clear at this time whether the small diameters of electrospun fibers are achieved as a result of a single filament undergoing a high degree of draw or through a splaying process similar to the Rayleigh disintegration described for electrospray.

Very little has been reported about the crystalline properties of electrospun fibers. This is of interest because polymer fibers used in high performance applications, such as Kevlar® and ultra-high molecular weight polyethylene, possess a high degree of crystallinity and crystal orientation. In 1981, Manley and Larrondo [18,19,20] electrospun a solution of polyethylene in paraffin at elevated temperatures. Based on reports by Baumgarten [17] of spinning velocities approaching the speed of sound, it was thought that the electrospinning process would have a high enough shear rate to produce polyethylene fibers with a highly oriented crystal structure. However, wide angle X-ray diffraction (WAXD) experiments revealed that the degree of orientation observed for the electrospun fibers was comparable to that of undrawn polyethylene fibers obtained from more conventional methods. More recent work by Srinivasen and Reneker [15] has shown that a reasonably high degree of crystal orientation can be obtained by electrospinning Kevlar® from sulfuric acid.

It is clear from the background literature for both the electrospray and electrospinning processes that the structure and morphology of the final product (be it particles or fibers) are determined by the effects of solution viscosity, surface tension, concentration, dielectric properties, the feed rate of the solution to the tip, and the acceleration voltage. For the specific case of electrospinning, most of the literature has explored the types of polymer solvent systems from which fibers can be produced. There has not been much work that addresses the effect of the variables previously mentioned on the submicron fiber structure and morphology. This is especially true for systems that undergo the splaying phenomena. The current work looks at the effect of solution concentration and accelerating voltage on the structure and morphology of submicron poly(ethylene oxide) (PEO) fibers obtained by electrospinning. It shows that profound changes in fiber diameter and morphology accompany changes in these variables. Analogies are drawn with similar experiments in electrospray literature to help analyze these results.

## 2. EXPERIMENTAL

The solutions used in the electrospinning experiments were prepared with 400,000 mol. wt. PEO purchased from Scientific Polymer Products. This material was dissolved in high pressure

liquid chromatography (HPLC) grade water. The mixture of PEO and water was heated to 60° C and agitated with a stir bar for approximately 24 hours. Concentrations ranged from 4% to 10%. Solution surface tensions for each solution were determined by the Wilhelmy Balance method using microscope cover glass slides that were cleaned with a butane torch. Solution viscosities were measured with a Thermal Analysis Instruments AR 1000-N constant stress rheometer in a cone and plate geometry. Each experiment was performed at 20° C with a 4-cm and 2° cone. Solutions were spun from a 50-ml gas chromatography syringe with a 23-gauge (diameter = 0.35 mm) needle. A Gamma High Voltage Research ES30P power supply was used to produce voltages ranging from 5.5 to 15.0 kV. Various electrically grounded materials, such as aluminum screen, were used as targets.

Electrospun fiber mats were analyzed using a Bruker D5005 diffractometer for WAXD experiments. Transmission WAXD experiments were performed with a Rigaku 18-kW rotating anode generator and Bruker Hi-Star 2D area detector. Melting temperatures and heats of fusion for the electrospun fiber mats were determined with a TA instruments differential scanning calorimeter (DSC). Morphological observations were made with a Phillips Electroscan environmental scanning electron microscopy (ESEM). The samples were held at a temperature of 4° C using a Peltier stage during the experiment to prevent beam damage to the sample.

The experimental setup for the study of the effect of concentration on electrospun fiber morphology was as follows. A 20- to 30-ml quantity of a PEO-water solution was placed in a 50-ml syringe. The syringe was then clamped in place to a ring stand that was 6.5 inches above a grounded target (metal screen). The power supply was connected to the metal syringe tip. Constant pressure in the form of a weight was applied to the syringe so that a small drop of solution was suspended in equilibrium above the target. The weight applied to syringe plunger was increased with increasing concentration in an attempt to achieve similar initial conditions. Once this equilibrium condition was achieved, a voltage of 7.0 kV was applied to the syringe tip to initiate the jet. Typical time to collect the mat was about 24 hours.

The physical setup for the study of the effect of voltage on nanofiber morphology was the same as that for the concentration study. A 20- to 30-ml quantity of 7% PEO-water solution was placed in the syringe, and the electrospinning process was performed for a number of voltages. The weight applied to the syringe plunger was kept constant for the entire experiment. Optical micrographs were taken with a Photometrics cooled charge coupled device (CCD) camera with 3,000 by 2,000 resolution. The camera was attached to a Questar Schmidt-Cassegrain telescope in order to achieve high magnification from a distance.

### 3. RESULTS AND DISCUSSION

#### 3.1 Nanofiber Morphology: Voltage Dependence

As discussed in the introduction, the initiating jet for the electrospray process occurs in a variety of modes. These modes occur at different voltages and have a significant effect on the droplet size distribution and current transport. Although distinct modes might be difficult to isolate and observe because of the high, nonlinear viscosity associated with most polymer solutions, instability of the initiating drop is expected to produce observable changes in the electrospun fiber morphology. For the case of electrospinning, it has been observed that the shape of the initiating drop changes with various spinning conditions (voltage, viscosity, feed rate) [17], but until recently [21], no relation between the initiating drop shape and fiber morphology was discussed.

In electrospray and electrospinning experiments, an electric current is associated with the process, which can be measured with a sensitive amperage meter. In effect, the droplets or fibers bridge the gap between the charged needle and the electrically grounded target, closing the circuit. In the case of electrospray, it has been shown that a change in the mode of spray initiation is accompanied by a corresponding change in the measured electrospray current.[9] In the case of electrospinning, the electric current attributable to the conduction of charge in the polymer solution can be assumed to be negligible.[17] The only mechanism of charge transport is the flow of polymer from the tip to the target. Therefore, an increase in the electrospinning current reflects an increase in the mass flow rate away from the tip when all other variables (conductivity, dielectric constant, and flow rate of solution to the tip) are held constant. Figure 2 is a plot of the spinning current as a function of voltage obtained during the experiment just described. It can be seen in this figure that the electrospinning current gradually increases with voltage in the 5- to 7-kV range. For voltages greater than 7 kV, a sharp increase in slope is observed, indicating that the electrospinning current increases more rapidly. The change in the slope of this plot that occurs at 7 kV coincides with the change in shape of the initiating drop seen in the optical micrographs (Figures 3 through 5) and also with the change in fiber morphology observed in the electron micrographs.

Figures 3 through 5 show electron micrographs of nanofiber mats and optical photos of the corresponding initiating jet for accelerating voltages 5.5, 7.0, and 9.0 kV. In Figure 3, the optical photograph shows a jet initiating from a solution drop suspended at the end of the syringe needle. This mode of jet initiation is similar in appearance to microdripping jet initiation mode reported in the electrospray literature [9], in which initiation occurs from a drop whose diameter is larger than

the capillary diameter. The jet initiates from a cone at the bottom of the drop that has a semi-vertical angle of  $50^\circ$ . This result is in good agreement with Taylor's theoretical prediction of  $49.3^\circ$  for a viscous fluid that exists in equilibrium in an electric field. The corresponding fiber mat shows fibers having a cylindrical morphology with just a very few nodular defects.

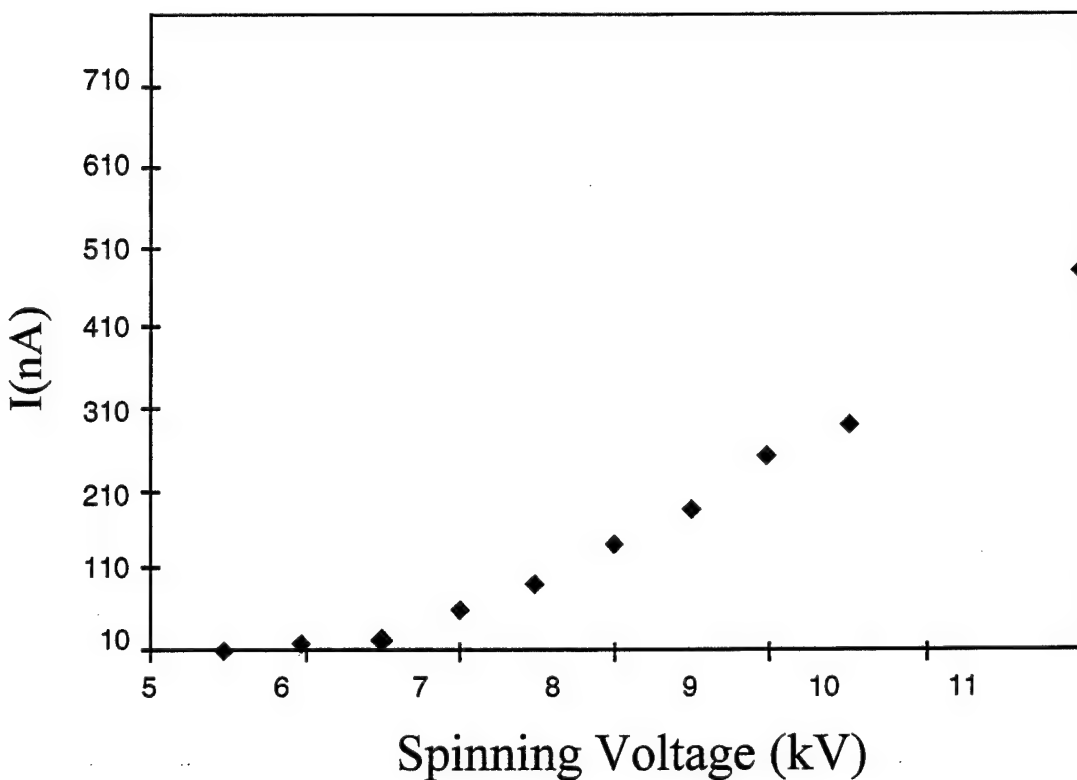
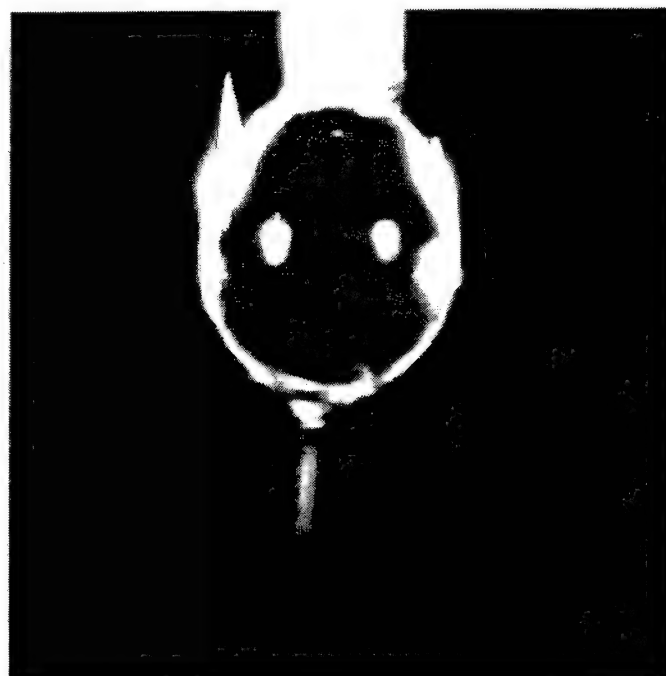


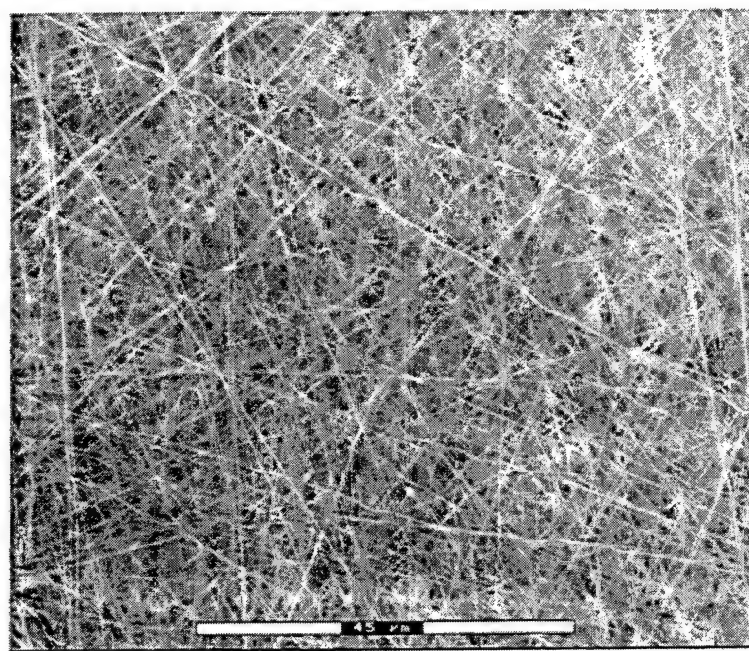
Figure 2. Electrospinning Current as a Function of Voltage.

At voltages of 7 kV or more, the jet initiates from within the capillary, rather than from a suspended drop or meniscus. At 7 kV, only the tip of the initiating cone is visible. The corresponding electrospun mat is composed of fibers with a cylindrical morphology and an increased number of nodule defects. At 9.0 kV, the solution jet is initiating directly from the tip with no meniscus in evidence. It is likely that the actual jet initiation occurs at some point inside the syringe needle for this case. The electron micrograph of the corresponding fiber shows that a very large number of nodule defects are present. Clearly, increasing the voltage increases the defect density significantly within the fiber mat. This phenomenon is quantified in Figure 6, which is a plot of defect density as a function of acceleration voltage, illustrating an order of magnitude increase in nodule defect density found in a nanofiber mat as the voltage is increased. From these

data, it is seen that the change in shape of the initiating drop at the syringe tip brought about by the increase in voltage is accompanied by a change in fiber morphology.

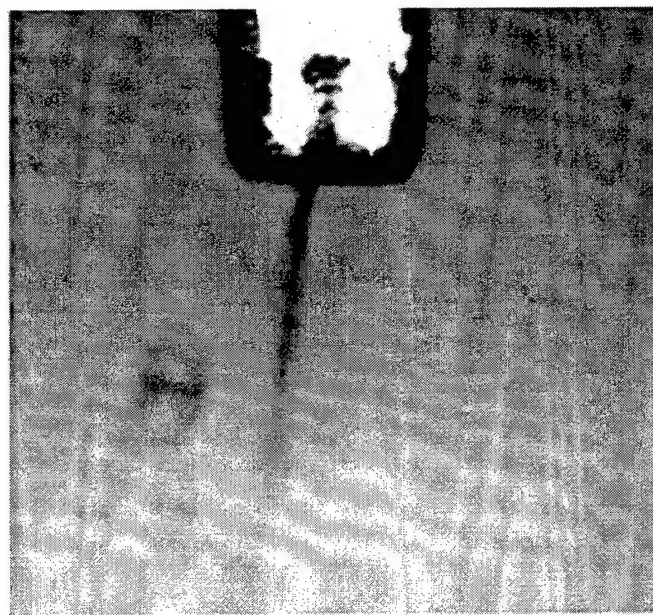


Initiating Jet: 5.5 kV

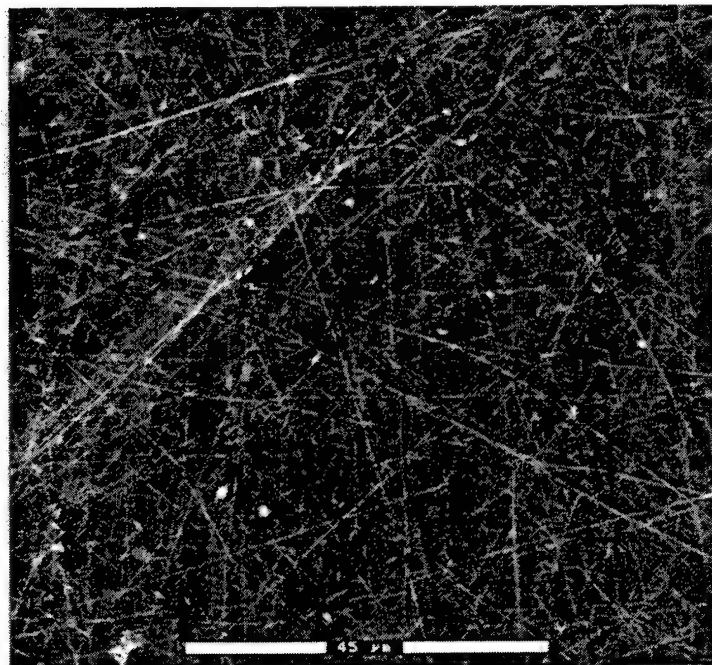


7% PEO Fiber Mat: 5.5kV

Figure 3. Initiating Cone and Corresponding Fiber Mat for a 7% PEO-Water Solution Spun at 5.5 kV.

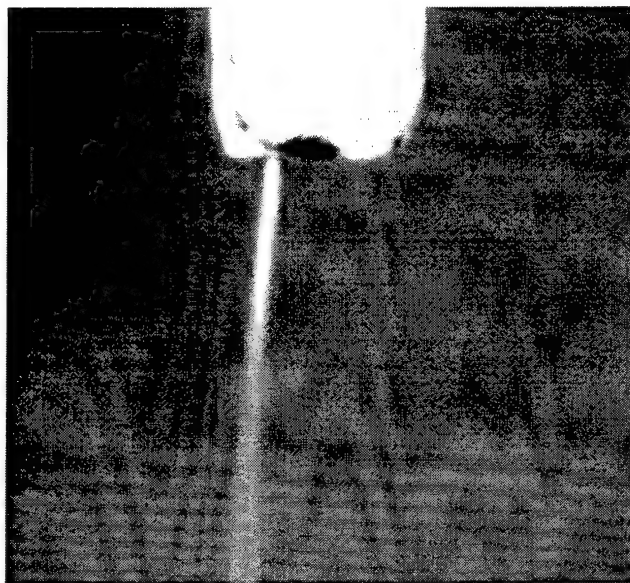


Initiating Jet: 7.0 kV

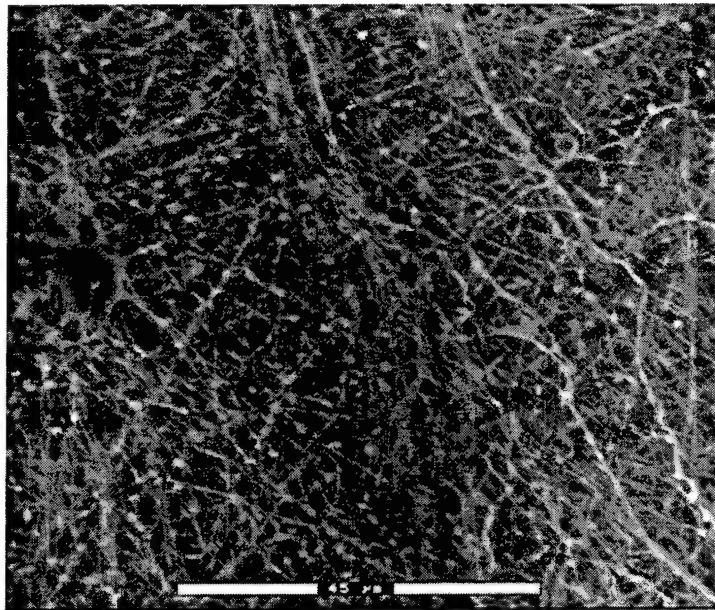


7% PEO Fiber Mat: 7.0 kV

Figure 4. Initiating Cone and Corresponding Fiber Mat for a 7% PEO-Water Solution Spun at 7.0 kV.



Initiating Jet: 9.0 kV



7% PEO Fiber Mat: 9.0 kV

Figure 5. Initiating Cone and Corresponding Fiber Mat for a 7% PEO-Water Solution Spun at 9.0 kV.

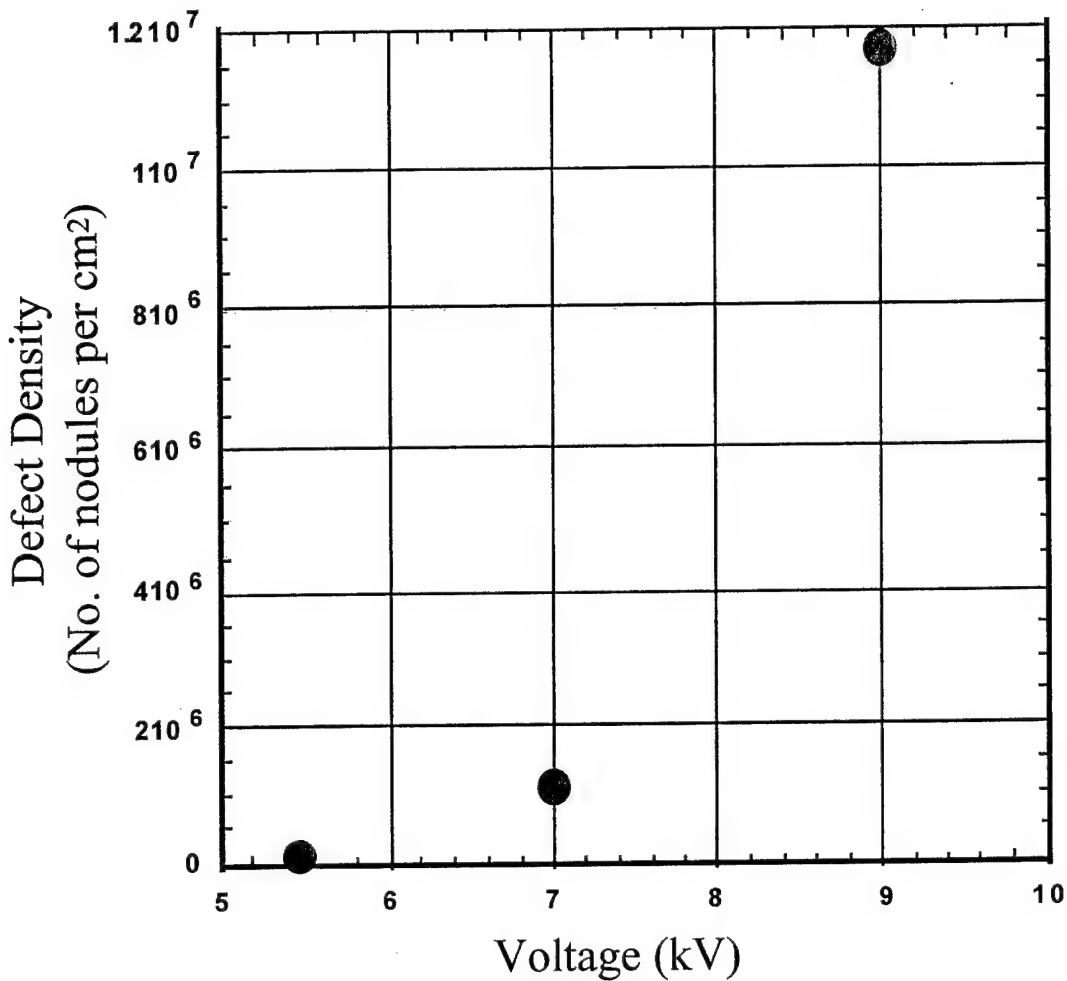


Figure 6. Node Density as a Function of Electrospinning Voltage.

In order for the initiating drop to form and maintain the equilibrium conical shape described by Taylor, it must maintain a minimum volume. Taylor demonstrated for the case of a meniscus on a static column of liquid that the volume of the conical meniscus will decrease upon formation of a jet. As the volume decreases, the shape of the meniscus oscillates and becomes asymmetrical, since it is no longer in equilibrium in the electric field. Eventually, the cone will collapse and the jet will be emitted from a flat surface. These results are analogous to those observed in the experiment described before. At 5 kV, the PEO-water solution is being fed to the tip of the syringe faster than the jet of polymer solution is carrying fluid away. As a result, a Taylor cone is maintained at the bottom of a large drop that acts as a reservoir. As the voltage is increased, the jet velocity increases and the solution is removed from the tip more quickly. At 7 kV, the drop at the tip of the needle has almost entirely disappeared, with only an apparent small fraction of a cone protruding from the syringe tip. This indicates that the solution is being removed faster than it is being supplied to the syringe tip. As the voltage is further increased, all that is seen is a jet that travels about the edge of the tip.

Observation of the shape of the initiating drop at higher voltages indicates that the initiating jet is unstable. This could result in large variations of the jet diameter, which in turn result in variations of final fiber diameter. In addition, the collapse of the initiating drop means that the polymer solution is being removed from the tip faster than it can be replaced. This means that at high voltages, the electrospinning jet undergoes a greater degree of strain than at lower voltages. Note that the mass flow rate away from the syringe tip is increased at higher voltages. This could mean that the electrospinning jet proceeds to the collection target more rapidly. In this case, it is likely that the collected fibers still retain solvent. Once collected on the target, the fibers are no longer under strain and under the influence of viscoelastic forces and surface tension; they relax, forming nodular defects connected by thin fibers.

### 3.2. Nanofiber Morphology: Concentration Dependence

It has been shown in the electrospray literature that solution concentration has a significant effect on the final size and distribution of particles. One of the goals of this work is to systematically explore the effect of concentration on the diameter and morphology of fibers electrospun from a PEO-water solution. All the results described in this section were obtained from fiber mats electrospun at a voltage of 7 kV onto an electrically ground target positioned 16.5 cm from the syringe tip. The range of concentrations examined in this study was 4% to 10% PEO in water. At concentrations below 4%, a mixture of fibers and droplets was generated by the electrospinning process, and it was not possible to collect a continuous fiber mat. Electrospinning from solutions with concentrations higher than 10% was prohibited by their high viscosity (see Figure 7). It was impossible to maintain an appropriate feed rate needed to produce a constant jet with the laboratory setup. Electron micrographs of fiber mats electrospun from 4% and 10% concentrations of PEO-water solutions are shown in Figure 8. These images demonstrate the two extremes in the fiber morphologies observed. In the micrograph of the fiber mat electrospun from a 4% solution of PEO, the fibers have an irregular, undulating morphology with large variations in diameter along a single fiber. There are numerous junctions and bundles of fibers. In the micrographs of the fiber mats electrospun from 10% PEO solutions, the nanofibers have a regular, cylindrical morphology, and on average, have a larger diameter that does not vary greatly along the length of the fiber.

The presence of junctions and bundles of fibers in the micrograph of the fiber mat electrospun from the 4% PEO solution is evidence that the polymer fibers are still wet at the time that they hit the collection screen. Since these wet fibers are no longer being strained after they are collected on the grounded target, they will deform as a result of surface tension and viscoelastic relaxation. The

result of this deformation is the undulating morphology seen in the micrograph of the 4% PEO solution fiber mat. At higher concentrations, the solution surface tension is greatly reduced and the fibers are mostly dry by the time they are collected on the target. These conditions result in the normal cylindrical fiber morphology and relatively few junctions seen in the micrograph of the fiber mat obtained from the 10% PEO solution.

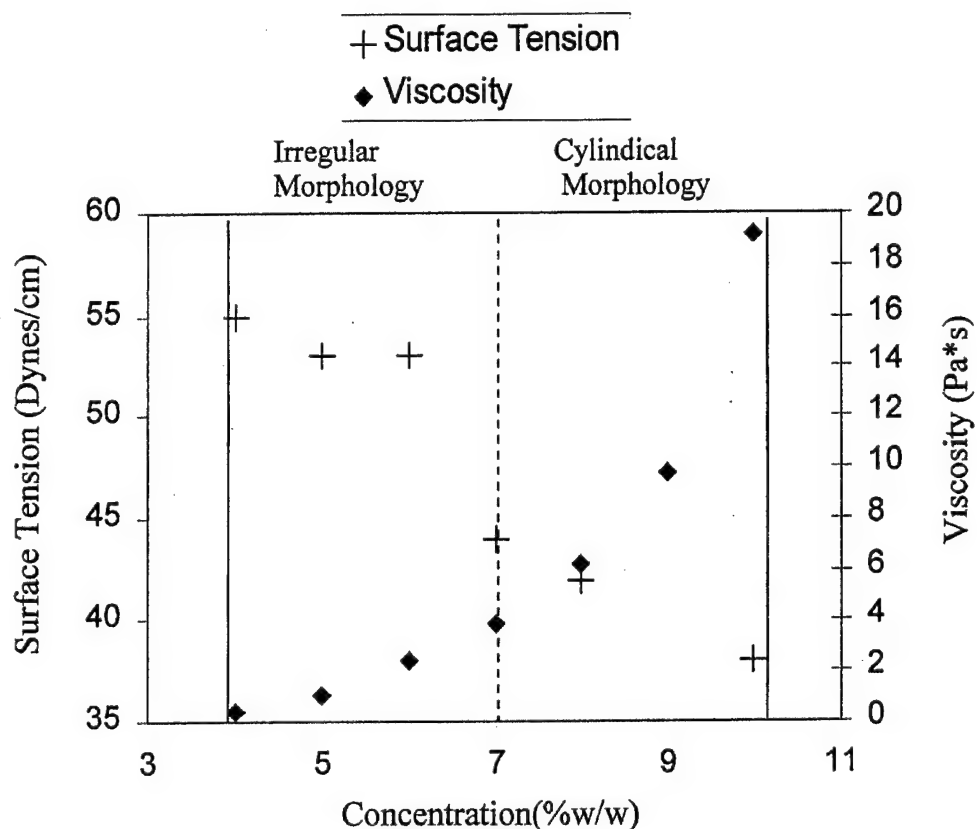


Figure 7. Concentration Dependence of Solution Surface Tension and Solution Viscosity for PEO-Water Solutions.

The effect of concentration on the average diameter of electrospun nanofibers is seen in the plot of the average fiber diameter as a function of PEO concentration shown in Figure 9. At solution concentrations  $\geq 8\%$ , the electrospun fiber mats exhibit a bimodal distribution (see Figure 10). This behavior is reminiscent of the bimodal droplet distribution that has been reported in electrospray literature and is the first time it has been reported for the electrospinning process. From Figure 9, it can be seen that the average diameter of the electrospun fibers corresponding to the primary distribution increases by the power of 0.53. Figure 11 is a plot of the percentage of fibers in the secondary distribution as a function of concentration. From this plot, it is seen that the fibers composing the secondary distribution become more significant in number at higher concentrations.

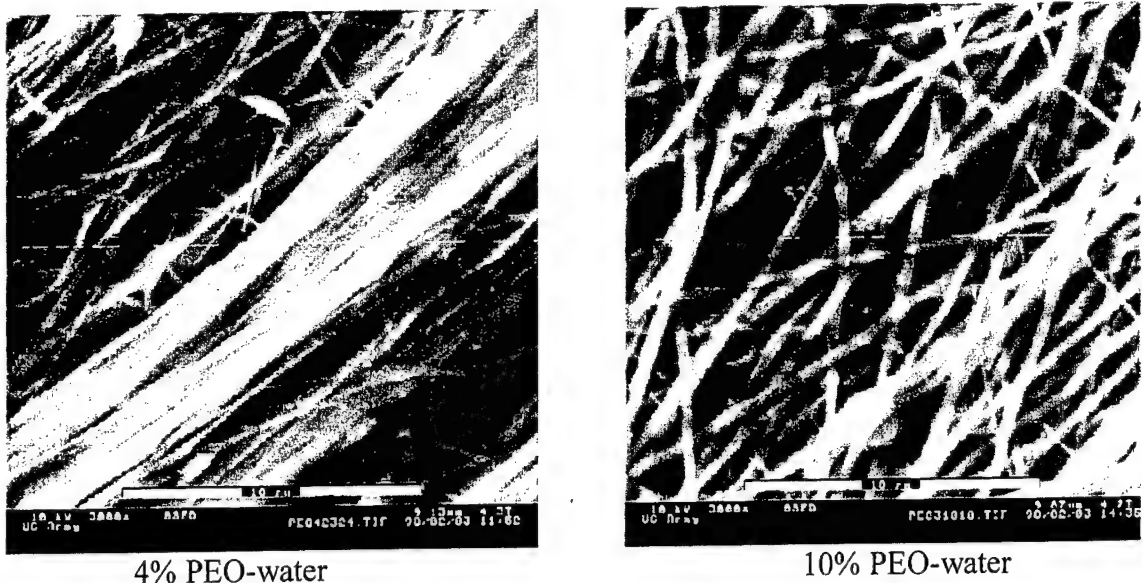


Figure 8. Electron Micrographs of Fiber Mats Electrospun From 4%, 7%, and 10% PEO-Water Solutions.

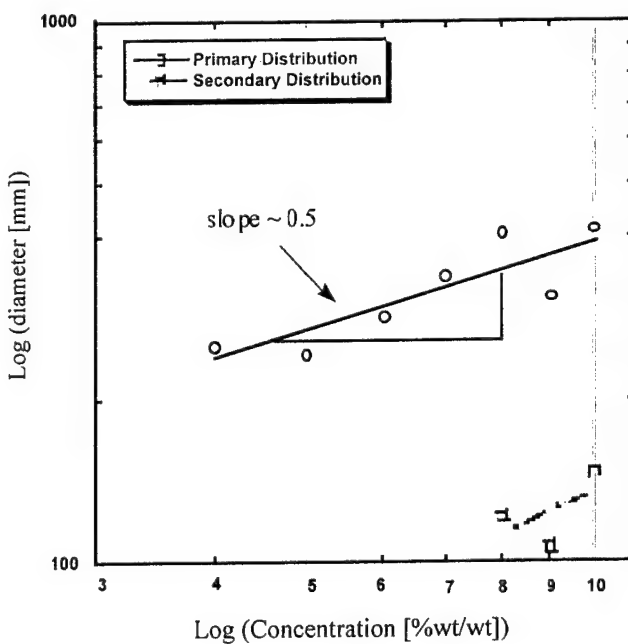


Figure 9. Average Fiber Diameter as a Function of PEO Concentration.

At this time, it is not entirely understood why the electrospinning process should exhibit a bimodal distribution at higher concentrations. Figure 12 shows two high-speed photographs of the electrospinning process for both 4% and 10% concentrations. For both cases, the voltage and distance to the ground plane were the same and the feed rate was approximately 0.5 ml/minute.

In the case of the 4% concentration solution, the path of the illuminated jet weaves its way laterally back and forth through a large volume as it is accelerated vertically toward the ground plane. In the picture corresponding to the 10% solution, the electrospinning jet appears to take a more direct path to the ground plane, and a small splay can be seen branching off the main jet. Although these pictures do not provide clear insight into the mechanism of splaying, it is evident that the increase in solution concentration causes a change in the path the electrospinning jet takes to ground and the distribution of splays along the jet. It is possible that the higher viscosity of the 10% PEO solution somehow causes the polymer jet to splay in an uneven fashion. However, further investigation into the fundamental mechanisms of the splaying process is needed in order to provide a satisfactory explanation for the observed bimodal distribution.

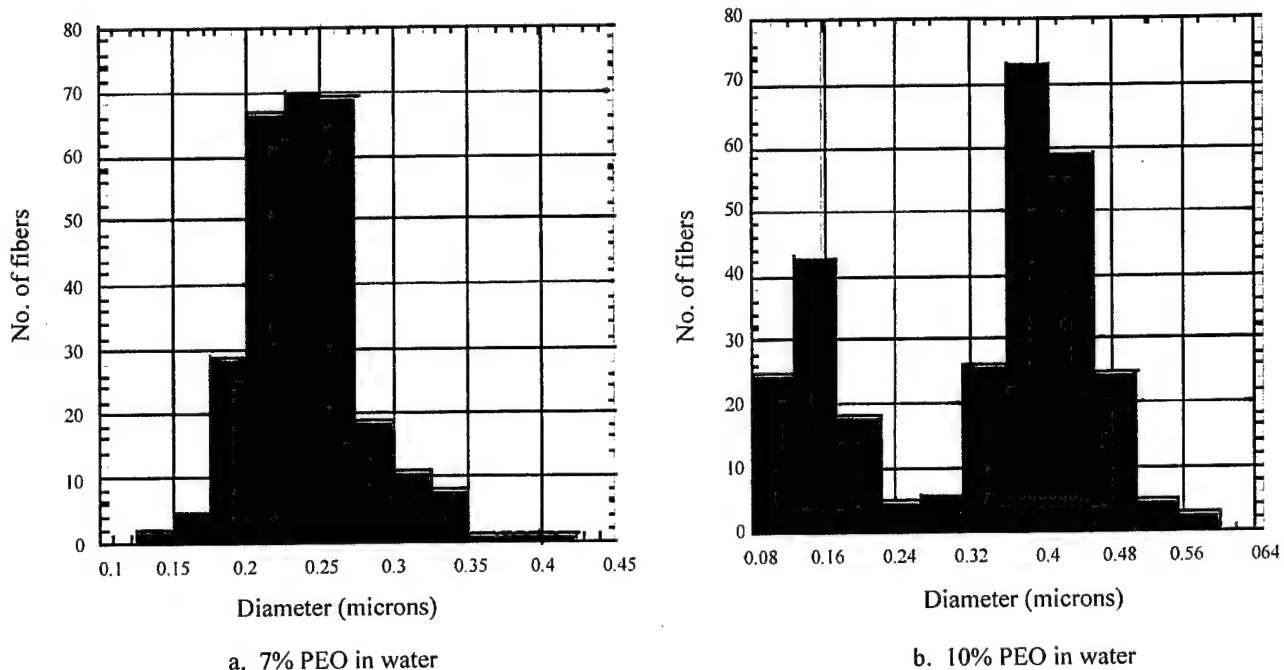


Figure 10. Bimodal Distribution of Fiber Diameters Electrospun From 7% and 10% PEO-Water Solution.

As stated in the introduction, there are numerous possible applications for this process involving filtration, which take advantage of the large amount of surface area that is available in non-woven mats composed of submicron fibers. Figure 13 is a plot of both the predicted and measured specific surface area for electrospun fiber mats as a function of spinning solution concentration. The predicted average specific surface area was calculated from the average fiber diameters reported earlier. This resulted in an increase of the average specific surface area at high concentrations (8% to 10%). The actual specific surface area of the electrospun fiber mats was

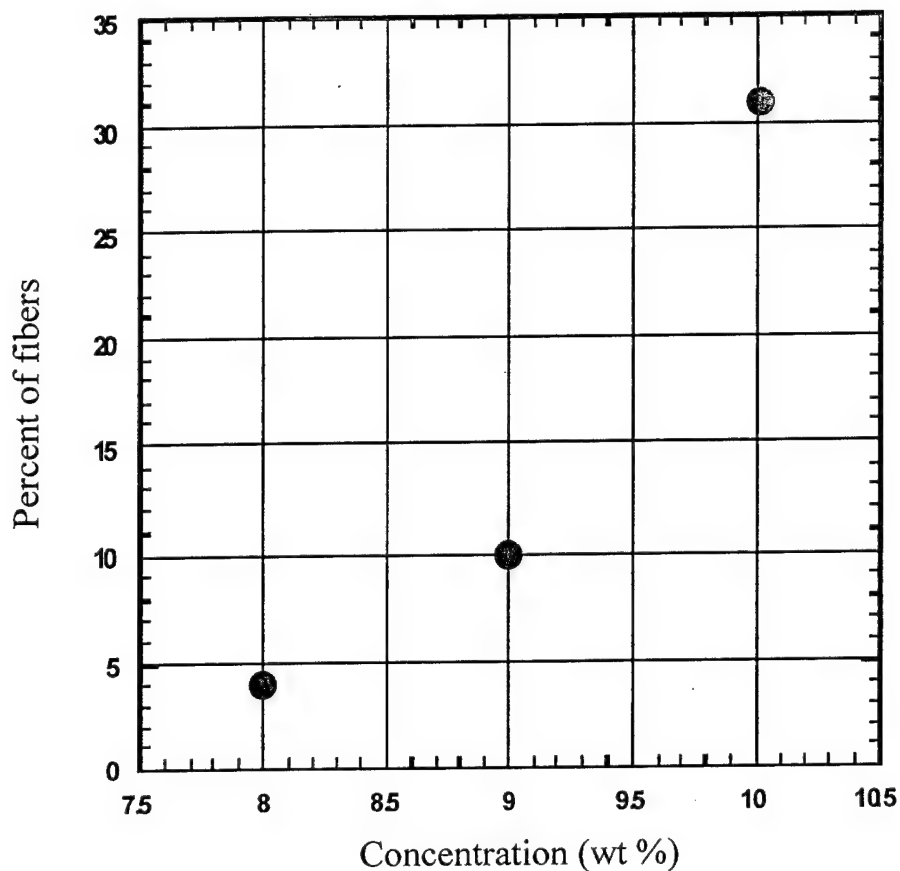


Figure 11. Percentage of Secondary Distribution as a Function of Concentration.

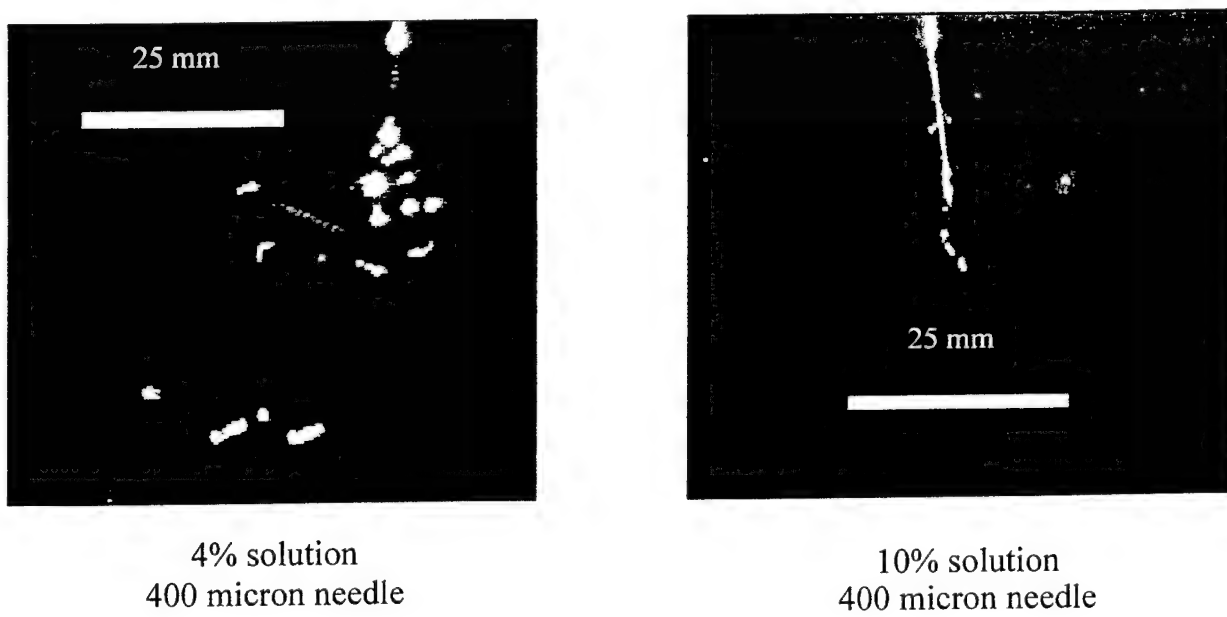


Figure 12. High Speed Photo-micrographs of the Electrospinning Process for 4% and 10% Solution Concentrations.

obtained through Brunauer-Emmett-Teller (BET) measurements. The measured specific surface areas for the fiber mats ranged from 10 to 20 square meters per gram. These values are several orders of magnitude higher than one would expect from textile fibers in the 10- to 20-micron range. Because of the small sample size, the error in the BET measurement was comparable to the magnitude of variation in the predicted specific surface area curve. Because of this, any attempt to compare trends between the predicted and measured curves would be meaningless. However, the fact that the predicted and measured values are of the same order of magnitude indicates that the average fiber diameter measurements presented here are representative of the whole fiber mat.

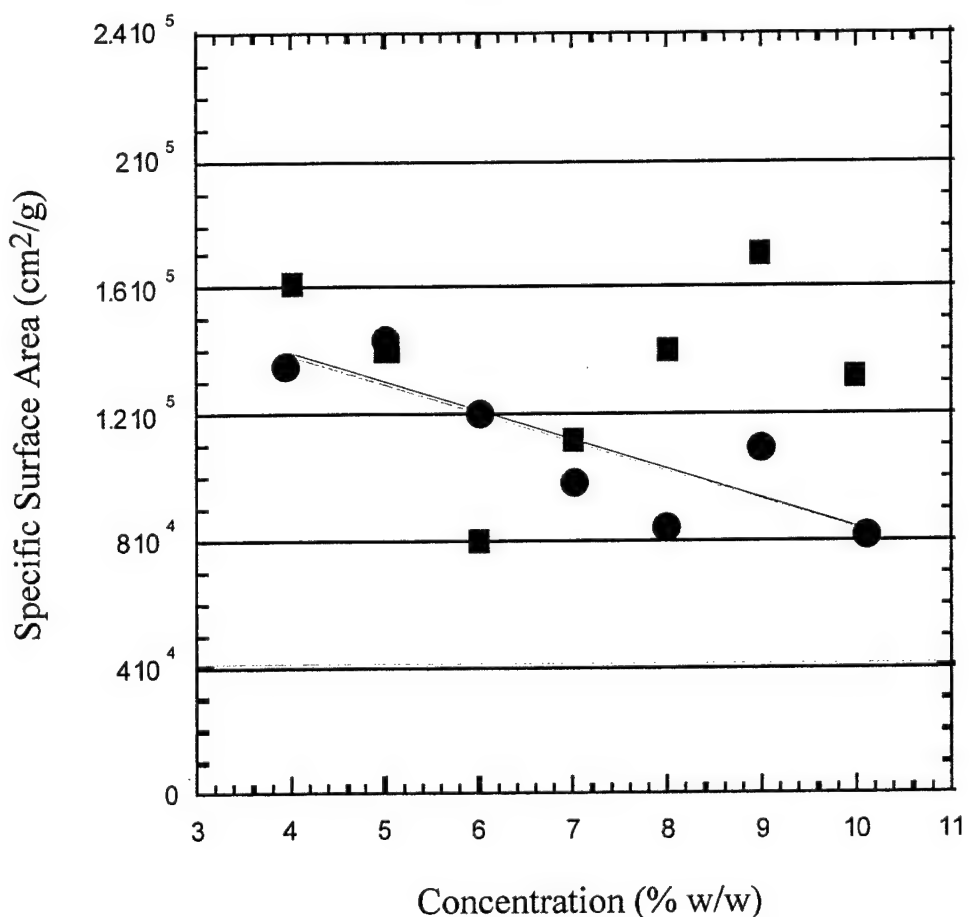


Figure 13. Specific Surface Area as a Function of Concentration.

### 3.3 General Characteristics of Electrospun Fibers and Fiber Mats

#### 3.3.1 *Crystallinity*

WAXD and DSC experiments have been performed with samples of PEO nanofiber mats electrospun from PEO-water solutions of different concentrations (4% to 10%). Figure 14 shows

WAXD patterns for both a PEO nanofiber mat spun from a 10% concentration PEO-water solution and the neat PEO powder from which the solution was made. From the figure, it is immediately evident that the diffraction peaks associated with the PEO powder are sharp and clearly defined, while the peaks in the pattern of the fiber mat are significantly broader and smeared together. From the Scherrer Equation,  $t=k\lambda/(\beta\cos\theta)$ , we know that the apparent crystallite size,  $t$ , is inversely proportional to the full width at half maximum (FWHM) of the diffraction peak. Therefore, the broader diffraction peaks associated with the PEO nanofiber mat indicate smaller, less perfect crystals than those in the neat PEO powder.

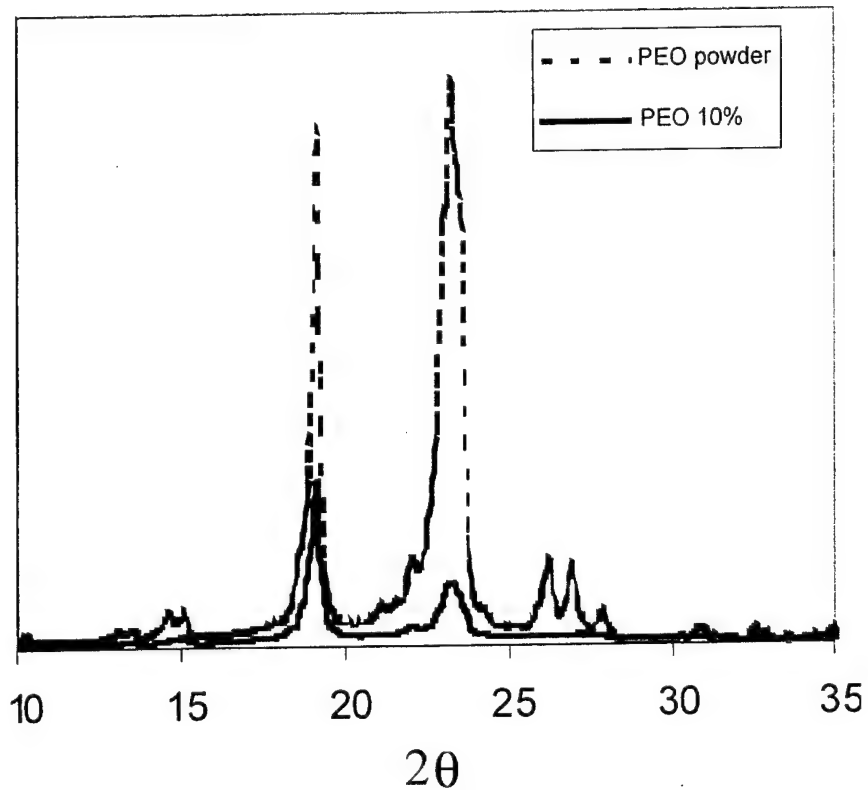


Figure 14. WAXD Patterns for PEO Powder and PEO Fiber Mat Electrosynthesized From 10% PEO-Water Solution.

The PEO fiber mat had a melting temperature,  $T_m$ , and heat of fusion,  $\Delta H_f$ , (66° C and 200 J/g) that were much lower than the  $T_m$  and  $\Delta H_f$  for the neat powder (71° C and 250 J/g). The lower heat of fusion and melting mean that the PEO fiber mat contains smaller, less perfect crystals than those in the neat PEO powder. This is consistent with the results from the WAXD experiments, indicating the crystallinity is not enhanced by the electrospinning process for the PEO-water solution.

### 3.3.2 Deposition of Nanofibers on a Substrate

During the course of our research, a number of observations have been made that suggest that during certain conditions, the residual charge left on the collected fibers affects how they will organize themselves in the non-woven mat. Specifically, the fibers will try to arrange themselves in such a way as to maximize contact with the electrically grounded target. Since many of the possible applications require a uniform distribution of fibers throughout a given area, these observations are presented in this section. Visual inspection of any electrospun fiber mat that has been collected on a metal screen will reveal that the mat is thicker at points in contact with the screen. For example, Figure 15a is an electron micrograph of a fiber mat spun from a 10% solution of PEO in water that has been collected on a wire screen. In this micrograph, the fiber mat is sitting over a junction of two wires in the screen. Although most of the fibers are primarily randomly oriented, numerous large filaments and ribbons on the surface of the mat are oriented along the length of one of the screen wires. At higher magnification (see Figure 15b), it is seen that these ribbons are actually composed of many smaller fibers that are oriented in the same direction and have adhered to each other.

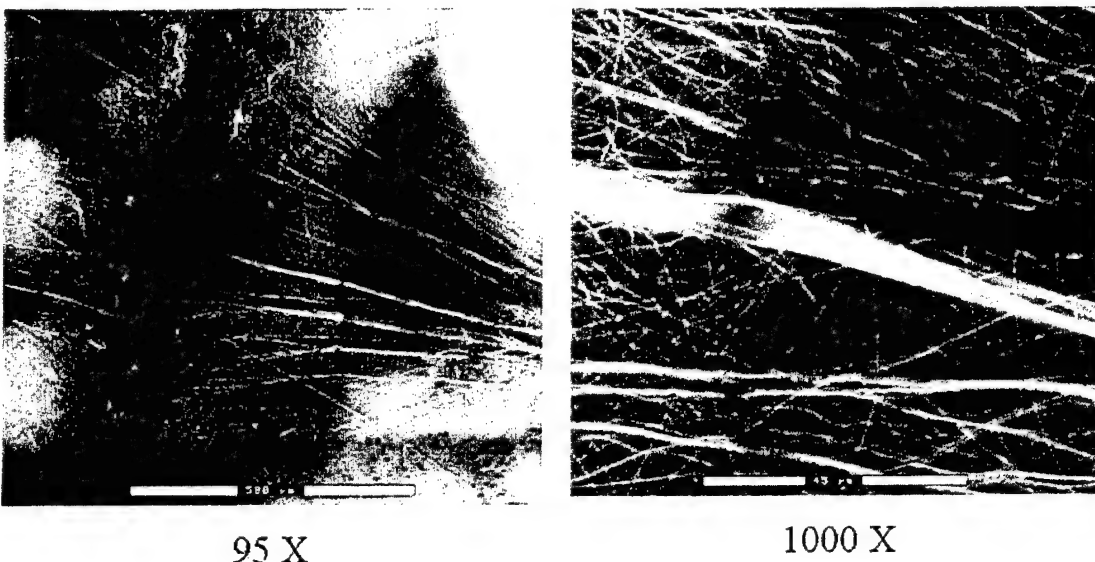


Figure 15. Fiber Mats Electrospun From 10% Solution of PEO in Water Collected Onto an Aluminum Screen.

Attempts to electrospin from solutions with low viscosities have resulted in a number of unusual, non-optimized morphologies. For example, Figure 16 is an optical micrograph of a 7% solution of 100,000 mol. wt. PEO in water that was electrospun onto an aluminum screen. In this case, the solution jet disintegrated into droplets, and polymer fibers never formed. The resulting morphology is a dendritic structure that radiates outward from the aluminum wire. Figure 17 is a

photo-micrograph of a screen on which material has been electrospun from a 2% solution of 400,000 mol. wt. PEO in water. Instead of a uniform non-woven fiber mat, the material has collected preferentially on the wires of the screen. Over time, the material has accumulated to form a three-dimensional representation of the screen. Since these fibers are most certainly still wet when they reach the target, it is likely that only fibers that are deposited along screen wire remain intact. Those fibers that try to span the distance between two screen wires break under the influences of surface tension and viscoelastic relaxation.

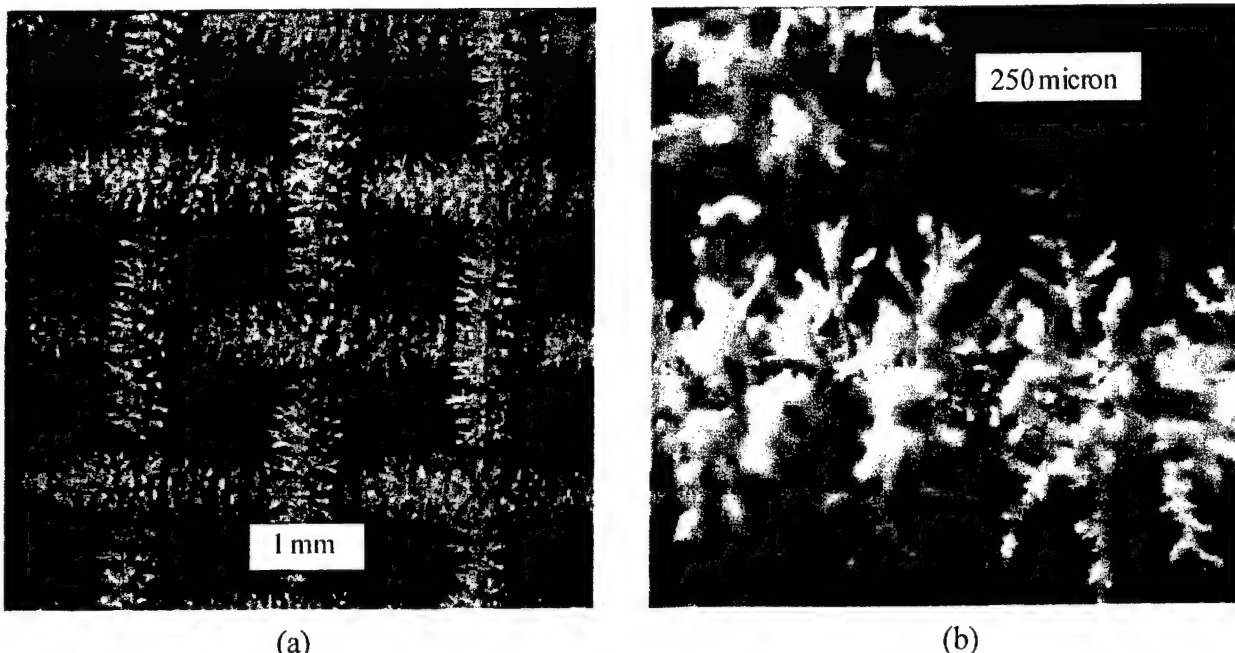


Figure 16. 7% Solution of 100,000 Mol. Wt. PEO in Water Electrosprayed Onto Aluminum Grid.

Three-dimensional fiber structures have also been observed in fiber mats collected on other types of substrates. Figure 18 is an electron micrograph of a fiber mat that has been electrospun from a 7% PEO-water solution at a voltage of 11 kV. It was collected on a piece of cloth that sat on top of a grounded piece of aluminum foil. Large ridges that form honeycomb-like structures on the surface of the electrospun are seen here. Figure 19a is a micrograph of one of these ridges at a higher magnification. The micrograph reveals a network of fibers on top of a blurred structure. By changing the working distance (i.e., focal plane) of the environmental electron microscope, it is possible to bring the background structure into focus. Figure 19b shows that this background structure is composed of a thick layer of polymer particles and fibers. Because of the high electrospinning voltage, the spinning rate is faster and the electrospun fibers are arriving at the cloth substrate wet and full of nodular defects. These nodules and fibers adhere to each other, forming the thick, continuous layer of polymer particles seen in Figure 18b. This layer of polymer eventually

accumulates enough of an electrostatic charge to prevent new electrospun fibers from lying directly on the mat. Instead, they are suspended slightly above the surface, where they have time to dry. The result is ridged honeycomb-like structure seen in Figure 18.

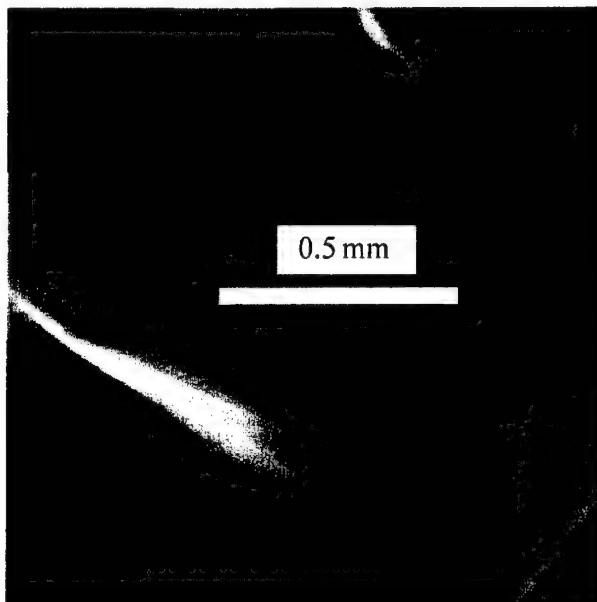


Figure 17. Photomicrograph of 2% PEO-Water Solution Electrospun Onto an Aluminum Grid.

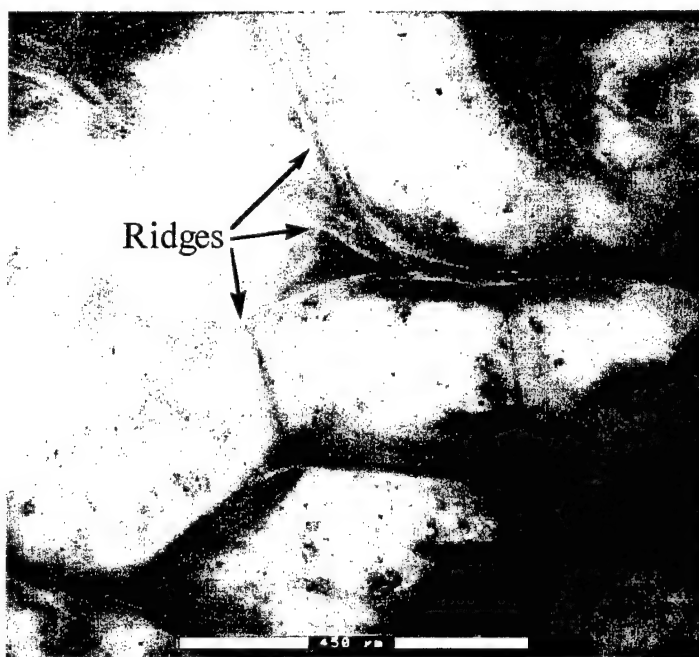


Figure 18. Three-dimensional Structure in Non-woven Fiber Mat Electrospun From a 7% Solution of 400,000 Mol. Wt. PEO and Water Electrospun at 11 kV Onto a Cloth Substrate.

All the examples given show that electrospun fibers (or electrospray drops) that reach an electrically grounded target carry enough residual charge to influence the morphology of the fiber mat. In each case, the electrospun material was deposited onto a stationary target. It is possible that these effects can be eliminated using different collection scenarios, such as electrospinning onto a rotating drum or using ions to remove the electrostatic charge from the fiber mat. For some applications, such as scaffolding for growing tissue cultures, the three-dimensional networks of submicron fiber might be of benefit.

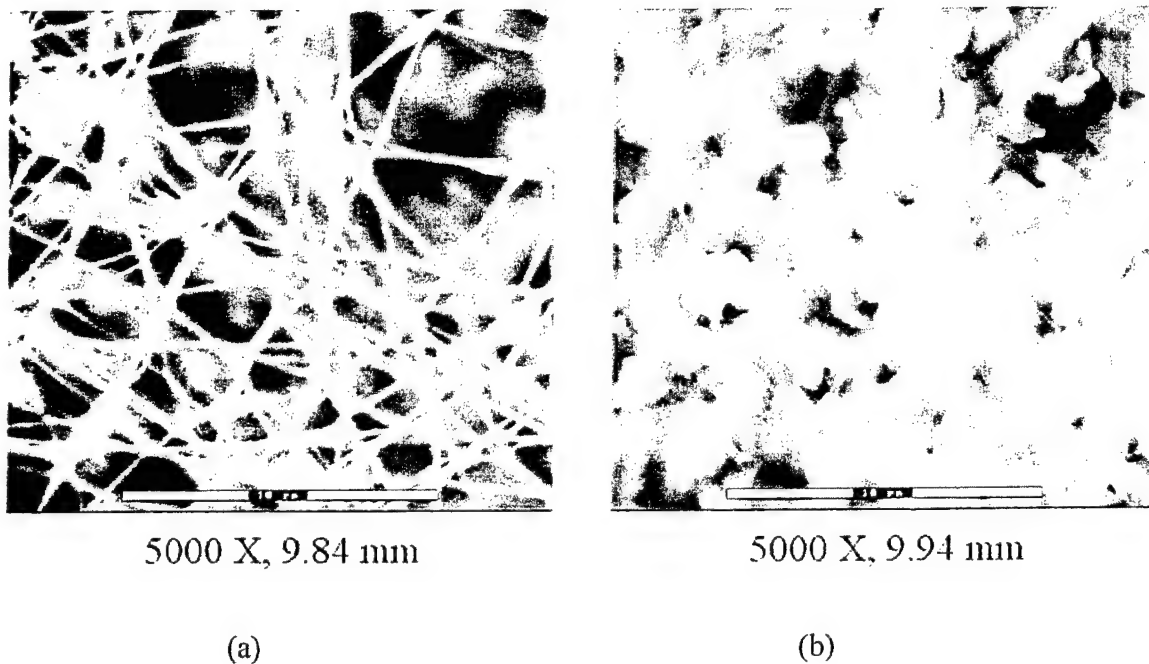


Figure 19. High Magnification Images of Figure 18 at Different Working Distances.

#### 4. CONCLUSIONS

This work has explored the effects of solution properties and processing parameters on the final structure and morphology of electrospun PEO nanofibers. The results presented here show that the morphology of electrospun nanofibers depends greatly on the feed rate of the polymer solution, the electrospinning voltage, the solution viscosity and surface tension, and the concentration of the solution. It has been shown that increasing the electrospinning voltage changes the shape of the initiating drop, which corresponds to a change in the fiber morphology from a typical cylindrical shape to the beaded or string-of-pearls morphology commonly observed.

Fibers electrospun from low concentration solutions (4%) have an irregular, undulating morphology, while fibers electrospun from higher concentration solutions (7% to 10%) have a regular, cylindrical morphology. The undulating morphology seen at low concentrations is the result of a combination of surface tension and viscoelastic relaxation of the wet fibers. At higher concentrations, the solution surface tension is decreased significantly and the fibers collected on the target are dry, so the morphology is cylindrical. It has been shown that the fiber diameter of the electrospun PEO increases as the 0.53 power with concentration. Further, at concentrations of 8% or higher, the fiber diameter exhibits a bimodal distribution. Although this behavior is similar to results reported for electrospray experiments, it is the first time it has been seen for electrospun polymer fibers.

Based on WAXD and DSC experiments, it has been shown that the electrospinning process does not significantly enhance the crystallinity or crystal structure of nanofibers spun from PEO-water solutions. It has been shown that electrospun fibers collected on a grounded target retain enough residual charge to influence the organization of the nanofibers in the non-woven mat. It has also been shown that in extreme cases, the surface of the non-woven mat will maintain a net static charge that will cause newly deposited fibers to organize and grow three-dimensional networks.

**INTENTIONALLY LEFT BLANK**

## REFERENCES

1. Dees, J.R., and J.E. Spruiell, *Journal of Applied Polymer Science*, 18, 1053-1078, 1974.
2. Barham, P.J., and A. Keller, *Journal of Materials Science*, 20, 2281-2302, 1985.
3. Gibson, P.W., H.L. Shreuder-Gibson, and D. Riven, *AIChE Journal*, 45, 190-195, 1999.
4. Zeleny, J., *Physical Review*, 3, 69-91, 1913.
5. Taylor, G. I., *Proceedings of the Royal Society of London, Series A*, 280, 383-397, 1964.
6. Taylor, G. I., *Proceedings of the Royal Society of London, Series A*, 313, 453-475, 1969.
7. Cloupeau, M., and B.J. Prunet-Foch, *Journal of Electrostatics*, 25, 165-184, 1990.
8. Grace, J.M., and J.C. M. Marijnissen, *Journal of Aerosol Science*, 25, 1005-1019, 1994.
9. Chen, D.R., D.Y.E. Pui, and S.L. Kaufman, *Journal of Aerosol Science*, 26, 963-977, 1995.
10. Gomez, A., and K. Tang, *Physics of Fluids*, 6, 404-414, 1994.
10. Gomez, A., and K. Tang, *Physics of Fluids*, 6, 2317-2325, 1994.
12. Fernandez de La Mora, J., and I.G. Loscertales, *Journal of Fluid Mechanics*, 260, 155-184, 1994.
13. Ganan-Calvo, A.M., *Journal of Aerosol Science*, 25, 309-310, 1994.
14. Reneker, D.H., and I. Chun, *Nanotechnology*, 7, 216-223,
15. Srinivasen, G., and D.H. Reneker, *Polymer International*, 36, 195-201, 1995.
16. Doshi, J., and D.H. Reneker, *Journal of Electrostatics*, 35, 151-160, 1995.
17. Baumgarten, P.K., *Journal of Colloid and Interface Science*, 36, 71, 1971.
18. Larrondo, L., and St.John Manley, *Journal of Polymer Science: Polymer Physics Edition*, 19, 909-920, 1981.
19. Larrondo, L., and St.John Manley, *Journal of Polymer Science: Polymer Physics Edition*, 19, 921-932, 1981.
20. Larrondo, L., and St.John Manley, *Journal of Polymer Science: Polymer Physics Edition*, 19, 933-940, 1981.
21. Fong, H., I. Chun, and D.H. Reneker, *Submitted to Polymer*, September 1998.

**INTENTIONALLY LEFT BLANK**

<u>NO. OF COPIES</u>	<u>ORGANIZATION</u>	<u>NO. OF COPIES</u>	<u>ORGANIZATION</u>
2	ADMINISTRATOR DEFENSE TECHNICAL INFO CENTER ATTN DTIC OCP 8725 JOHN J KINGMAN RD STE 0944 FT BELVOIR VA 22060-6218	1	US ARMY RD&E CENTER ATTN T TASSINARI NATICK MA 01760-5020
1	DIRECTOR US ARMY RESEARCH LABORATORY ATTN AMSRL CS AL TA REC MGMT 2800 POWDER MILL RD ADELPHI MD 20783-1197	1	LOS ALAMOS NATL LAB ATTN DE QUAN LI MS-G755 CST-4 PO BOX 1663 LOS ALAMOS NM 87545
1	DIRECTOR US ARMY RESEARCH LABORATORY ATTN AMSRL CI LL TECH LIB 2800 POWDER MILL RD ADELPHI MD 207830-1197	1	NIST POLYMERS RESEARCH ATTN CHARLIE GUTTMAN BLDG 224 GAIITHERSBURG MD 20899
1	DIRECTOR US ARMY RESEARCH LABORATORY ATTN AMSRL DD JJ ROCCHIO 2800 POWDER MILL RD ADELPHI MD 20783-1197	1	US ARMY SOLDIER SYSTEMS CMD US ARMY NATICK RD&E CENTER ATTN SSCNC IP QUOC TRUONG KANSAS STREET NATICK MA 01760-5019
5	US ARMY NATICK RD&E CENTER ATTN SSCNC YM HEIDI GIBSON NATICK MA 01760-5020	1	DUPONT NYLON FIBER ENGINEERING TECH CTR ATTN JAYESH DOSHI 4501 ACCESS ROAD CHATTANOOGA TN 37415
1	US ARMY RD&E CENTER ATTN PHIL CUNNIFF NATICK MA 01760-5020	1	UNIV OF CONNECTICUT CHEMICAL ENGINEERING DEPT ATTN JEFF KOBERSTEIN 191 AUDITORIUM ROAD U-222 STORRS CT 06269-3222
1	PROF DAVE MARTIN 2541 CHEMISTRY BUILDING 930 N UNIVERSITY AVE ANN ARBOR MI 48109-1055	5	UNIV OF ILLINOIS URBANA-CHAMPAIGN DEPT OF CHEMICAL ENGINEERING ATTN PROF TONY MCHUGH ROGER ADAMS LABORATORY MC-712 600 SOUTH MATHEWS AVENUE URBANA IL 61801-3792
1	STATE UNIV OF NEW YORK AT STONY BROOK CHEMISTRY DEPT ATTN PROF BEN HSIAO STONY BROOK NY 11794-3400	1	FOSTER-MILLER ATTN WALTER ZUCKUS 103 BEAR HILL RD WALTHAM MA 02154-1196
1	MASSACHUSETTS INST OF TECH DEPT OF CHEMICAL ENGINEERING ATTN PROF GREG RUTLEDGE CAMBRIDGE MA 02139-4307	1	UNIV OF NORTH CAROLINA CHAPEL HLL CHEMISTRY DEPARTMENT ATTN JOE DESIMONE 211 VENABLE HALL CB #3290 CHAPEL HILL NC 27599-3290
1	US ARMY RD&E CENTER ATTN DON RIVIN NATICK MA 01760-5020		

<u>NO. OF COPIES</u>	<u>ORGANIZATION</u>	<u>NO. OF COPIES</u>	<u>ORGANIZATION</u>
5	THE UNIVERSITY OF AKRON GOODYEAR INST OF POLYMER SCIENCE ATTN DARRELL RENEKER AKRON OH 44325-3909	1	US ARMY TANK-AUTOMOTIVE & ARMAMENTS CMD ATTN AMSTA AR TD M FISSETTE BLDG 1 PICATINNY ARSENAL NJ 07806-5000
1	DOD JOINT CHIEFS OF STAFF ATTN J39 CAPABILITIES DIV CAPT J M BROWNELL THE PENTAGON RM 2C865 WASHINGTON DC 20301	1	US ARMY TANK-AUTOMOTIVE CMD RD&E CTR ATTN AMSTA TA J CHAPIN WARREN MI 48397-5000
1	OFC OF THE SECY OF DEFNS ATTN ODDRE (R&AT) G SINGLEY THE PENTAGON WASHINGTON DC 20301-3080	1	US ARMY TRAINING & DOCTRINE CMD BATTLE LAB INTEGRATION & TECH DIR ATTN ATCD B J A KLEVECZ FT MONROE VA 23651-5850
1	OSD (no classified) ATTN OUSD(A&T)/ODDDR&E(R) ATTN R J TREW THE PENTAGON WASHINGTON DC 20310-0460	1	NAV SURFACE WARFARE CTR ATTN CODE B07 J PENNELLA 17320 DAHLGREN RD BLDG 1470 RM 1101 DAHLGREN VA 22448-5100
1	AMCOM MRDEC ATTN AMSMI RD W C MCCORKLE REDSTONE ARSENAL AL 35898-5240	1	DARPA ATTN B KASPAR 3701 N FAIRFAX DR ARLINGTON VA 22203-1714
1	CECOM ATTN PM GPS COL S YOUNG FT MONMOUTH NJ 07703	1	UNIV OF TEXAS ARL ELECTROMAG GROUP CAMPUS MAIL CODE F0250 ATTN A TUCKER AUSTIN TX 78713-8029
1	CECOM SP & TERRESTRIAL COMMCTN DIV ATTN AMSEL RD ST MC M H SOICHER FT MONMOUTH NJ 07703-5203	1	HICKS & ASSOCIATES, INC. ATTN G SINGLEY III 1710 GOODRICH DR STE 1300 MCLEAN VA 22102
1	US ARMY INFO SYS ENGRG CMND ATTN ASQB OTD F JENIA FT HUACHUCA AZ 85613-5300	1	SPECIAL ASST TO THE WING CDR 50SW/CCX CAPT P H BERNSTEIN 300 O'MALLEY AVE STE 20 FALCON AFB CO 80912-3020
1	US ARMY NATICK RDEC ACTING TECHNICAL DIR ATTN SSCNC T P BRANDLER NATICK MA 01760-5002	1	HQ AFWA/DNX 106 PEACEKEEPER DR STE 2N3 OFFUTT AFB NE 68113-4039
1	US ARMY RESEARCH OFC 4300 S MIAMI BLVD RESEARCH TRIANGLE PARK NC 27709		<u>ABERDEEN PROVING GROUND</u>
1	US ARMY SIMULATION TRAIN & INSTRMNTN CMD ATTN J STAHL 12350 RESEARCH PARKWAY ORLANDO FL 32826-3726	2	DIRECTOR US ARMY RESEARCH LABORATORY ATTN AMSRL CI LP (TECH LIB) BLDG 305 APG AA

NO. OF  
COPIES ORGANIZATION

1 US ARMY RESEARCH LABORATORY  
ATTN AMSRL WM M GARY HAGNAUER  
BLDG 4600  
APG MD 21005-5069

25 US ARMY RESEARCH LABORATORY  
ATTN AMSRL WM MA  
JOE DEITZEL (20 CYS)  
NORA BECK TAN (5 CYS)  
BLDG 4600  
APG MD 21005-5069

7 CBDCOM  
ATTN DAVID TEVAULT (5 CYS)  
ERICA VALDEZ  
JEFF HALE  
EDGEWOOD RD&E CENTER  
BLDG  
5232 FLEMING RD  
APG MD 21010-5423

ABSTRACT ONLY

1 DIRECTOR  
US ARMY RESEARCH LABORATORY  
ATTN AMSRL CS AL TP TECH PUB BR  
2800 POWDER MILL RD  
ADELPHI MD 20783-1197

INTENTIONALLY LEFT BLANK

# REPORT DOCUMENTATION PAGE

Form Approved  
OMB No. 0704-0188

Public reporting burden for this collection of information is estimated to average 1 hour per response, including the time for reviewing instructions, searching existing data sources, gathering and maintaining the data needed, and completing and reviewing the collection of information. Send comments regarding this burden estimate or any other aspect of this collection of information, including suggestions for reducing this burden, to Washington Headquarters Services, Directorate for Information Operations and Reports, 1215 Jefferson Davis Highway, Suite 1204, Arlington, VA 22202-4302, and to the Office of Management and Budget, Paperwork Reduction Project (0704-0188), Washington, DC 20503.

1. AGENCY USE ONLY (Leave blank)	2. REPORT DATE	3. REPORT TYPE AND DATES COVERED	
	June 1999	Final	
4. TITLE AND SUBTITLE  Generation of Polymer Nanofibers Through Electrospinning			5. FUNDING NUMBERS  PR: 611102AH42
6. AUTHOR(S)  Deitzel, J.M. ; Beck Tan, N.C.; Kleinmeyer, J.D. (all of ARL); Rehrmann, J.; Tevault, D. (both of ECBC); Reneker, D. (Univ of Akron); Sendijarevic, I.; McHugh, A. (both of Univ of Illinois)			
7. PERFORMING ORGANIZATION NAME(S) AND ADDRESS(ES)  U.S. Army Research Laboratory Weapons & Materials Research Directorate Aberdeen Proving Ground, MD 21010-5066		8. PERFORMING ORGANIZATION REPORT NUMBER	
9. SPONSORING/MONITORING AGENCY NAME(S) AND ADDRESS(ES)  U.S. Army Research Laboratory Weapons & Materials Research Directorate Aberdeen Proving Ground, MD 21010-5066		10. SPONSORING/MONITORING AGENCY REPORT NUMBER  ARL-TR-1989	
11. SUPPLEMENTARY NOTES			
12a. DISTRIBUTION/AVAILABILITY STATEMENT  Approved for public release; distribution is unlimited.		12b. DISTRIBUTION CODE	
13. ABSTRACT (Maximum 200 words)  Non-woven fabrics composed of nanofibers have a large specific surface area and small pore size compared to commercial textiles. These properties make such non-woven fabrics excellent candidates for filter and membrane applications, particularly in the areas of chemical and biological agent defense. Nanofibers may be produced by electrospinning, which uses an electric field to produce continuous fibers with diameters in the tens of nanometers range. Although the technique has been known for some time, very little information concerning the effect of processing variables such as solution concentration, viscosity, surface tension, flow rate and acceleration voltage on final fiber properties exists in the literature. In this work, nanofibers of polyethylene oxide have been electrospun from a range a solution concentrations and for a range of voltages. Wide angle X-ray diffraction and differential scanning calorimetry indicate that crystal structure is poorly developed in the electrospun fibers, when compared to results obtained from poly(ethylene oxide) powder. Fiber diameter increases with increasing concentration by the 0.53 power. We find that for concentrations of 8% (wt) and greater, a bimodal fiber diameter distribution has been observed, which is analogous to results reported for electrospray experiments. The density of node defects has been shown to increase with increasing voltage for a constant solution feed rate.			
14. SUBJECT TERMS  electrospinning      PEO nanofibers		15. NUMBER OF PAGES 40	16. PRICE CODE
17. SECURITY CLASSIFICATION OF REPORT Unclassified	18. SECURITY CLASSIFICATION OF THIS PAGE Unclassified	19. SECURITY CLASSIFICATION OF ABSTRACT Unclassified	20. LIMITATION OF ABSTRACT